Neutral Pion Photoproduction in a Regge Model

V. Mathieu*

Center for Exploration of Energy and Matter, Indiana University, Bloomington, IN 47403 and
Physics Department, Indiana University, Bloomington, IN 47405

G. Fox

School of Informatics and Computing, Indiana University, Bloomington, IN 47405, USA

A. P. Szczepaniak

Center for Exploration of Energy and Matter, Indiana University, Bloomington, IN 47403
Physics Department, Indiana University, Bloomington, IN 47405 and
Thomas Jefferson National Accelerator Facility, Newport News, VA 23606, USA

(Dated: May 4, 2015)

The reaction $\gamma p \to \pi^0 p$ is investigated in the energy range above the resonance region. The amplitudes include the leading Regge singularities in the cross-channel and correctly describe the differential cross section for beam energies above 4 GeV and for momentum transferred above -3 GeV^2. The energy dependence of the beam asymmetry and the reaction $\gamma n \to \pi^0 n$ seem is quantitative consistent with the Regge-pole dominance.

I. INTRODUCTION

Single pion photoproduction on a nucleon is one of the key reactions in hadron physics. At low energies, it is used to excite nucleon resonances while at high energies it can be used to test predictions of Regge theory, *e.g.* factorization of Regge poles [1]. The two regimes are analytically connected and relations *e.g.* finite energy sum rules (FESR), can be derived to constrain resonance parameters by the cross-channel Reggeons [2]. In recent years the CLAS experiment at JLab collected data on single pion production using photon beams with energies ranging from $E_\gamma = 1.275$ GeV to 5.425 GeV [3]. This energy range overlaps with both, the resonance and the Regge regions. Once the data is analyzed it will open the possibility to perform finite energy sum rules studies of pion photoproduction based on data from a single experiment. This will reduce systematic uncertainties and possibly help to clarify some of the outstanding theoretical issues encountered in earlier studies [4]. Single pion photoproduction will also be among the first reactions studied with the newly completed GlueX detector that will use highest energy photons from the recently upgraded CEBAF accelerator.

There are several pion photoproduction models developed to describe the nucleon resonance region [5–8], which is not the case of the high-energy regime. In view of the forthcoming measurements it is therefore necessary to revisit the theoretical models. This the main focus of this paper. According to Regge theory, at asymptotically large center of mass energies reaction amplitudes are determined by the right-most singularly in the complex angular momentum plane of the cross-channel partial waves. Except for elastic scattering, which is dominated by the Pomeron, these are the Regge poles. A single Regge pole contribution factorizes into a product of "couplings/residues" and "propagators". This property enables classification of Regge poles similar to that of elementary particles [9]. As the center of mass energy decreases, sub-leading angular momentum plane singularities become relevant including Regge poles with lower intercept *aka.* daughter trajectories and Regge cuts. Since the ultimate goal is to connect the Regge and resonance regions and make predictions for the energy range of the CLAS measurement, in this paper we also explore these sub-leading contributions. We focus on scattering in the forward direction where the dominant Regge singularities originate from the $t-$channel exchanges. The goal is to find a simple, albeit consistent with Regge theory, parametrization that once the CLAS data is analyzed, can be applied in a simultaneous study of the resonance and Regge regions *e.g.* using finite energy sum rules.

The paper is organized as follows. In Section II we discuss the t-channel amplitudes and their connection to the direct, s-channel observables. Conventions and details of calculations are given in Appendix A and B. Specification of the Regge exchange model is given in Section III. Analysis of existing data is summarized in Section IV and predictions for the CLAS energy range and for $E_\gamma = 9$ GeV, relevant for the upcoming experiments at JLab are given in Section V. Conclusions are summarized in Section VI.

II. FORMALISM

The reaction $\gamma(k, \lambda)N(p_2) \to \pi(q)N(p_4)$ describing pion with momentum q, the photon with momentum k and helicity λ, and a pair of nucleons with momenta p_2 and p_4 is given in terms of four invariant amplitudes, which are linearly related to four helicity amplitudes. The scalar amplitudes are functions of two independent

---
* mathieuv@indiana.edu

Mandelstam variables, $s = (k + p_2)^2$ and $t = (k - q)^2$. The helicity amplitudes are frame dependent. The two relevant frames for our discussion are the $s-$channel and $t-$channel frames. They correspond to the center of mass frame of the reaction $\gamma N \to \pi^0 N$ for the $s-$channel and $\gamma \pi^0 \to \bar{N}N$ for the $t-$channel, respectively. Helicity amplitudes in the $s-$channel are used to compute observables. At high energies and small scattering angles the s-channel amplitudes are dominated by singularities in the complex angular plane of the $t-$channel. Helicity amplitudes in the $t-$channel are therefore needed to identify the allowed Regge exchanges. Detailed analysis of the $t-$channel helicity amplitudes and their quantum numbers is given in Appendix A. The $s-$channel helicity amplitudes and the observables are discussed in Appendix B. In this section we summarize the main results.

The invariant amplitudes, $A_i(s,t)$ multiply four independent tensors constructed from the photon polarization vector, two Dirac spinors and particle momenta constrained to fulfill global symmetry requirements and gauge invariance. The tensors are conventionally chosen from the Chew-Goldberger-Low-Nambu (CGLN) basis [10], and the helicity amplitudes are given by

$$A^s_{\mu_4,\mu_2\mu_1}(s,t) = \bar{u}_{\mu_4}(p_4) \sum_{i=1}^{4} A_i(s,t) M_i \, u_{\mu_2}(p_2), \quad (1a)$$

$$A^t_{\lambda_4\lambda_2,\lambda_1}(s.t) = \bar{u}_{\lambda_4}(p_4) \sum_{i=1}^{4} A_i(s,t) M_i v_{\lambda_2}(-p_2), \quad (1b)$$

with the subscripts s and t referring to the s and t channels, and in the following we use μ_i and λ_i to denote particle helicities in the two channels. The tensors M_i are given in (A2). The scalar functions A_i have dynamical singularities in s and t while the helicity amplitudes have additional singularities arising from the kinematical factors in Eq. (1). To identify t-channel reggeons it is necessary to identify t-channel helicity amplitudes free from kinematical singularities. Kinematical singularities are related to presence of spin and can be related to singularities of the Wigner-d functions. The rotational functions can be written as $d^J_{\lambda'\lambda}(z_t) = \xi_{\lambda'\lambda}(z_t) P^J_{\lambda'\lambda}(z_t)$ where P^J is a polynomial and

$$\xi_{\lambda'\lambda}(z_t) = \left(\frac{1-z_t}{2}\right)^{\frac{1}{2}|\lambda'-\lambda|} \left(\frac{1+z_t}{2}\right)^{\frac{1}{2}|\lambda'+\lambda|}, \quad (2)$$

with $\lambda = \lambda_1 - \lambda_3 = \lambda_1$, $\lambda' = \lambda_2 - \lambda_4$. As shown in Appendix A singularities in s of the t-channel helicity amplitudes can be removed by dividing helicity amplitudes by ξ,

$$\hat{T}_{\lambda'\lambda} = \xi^{-1}_{\lambda'\lambda}(z_t) A^t_{\lambda_4\lambda_2,\lambda_1}(s,t). \quad (3)$$

The remaining singularities of $\hat{T}$ in s are dynamical in nature. Since reggeons have well defined quantum numbers in the $t-$channel, they will contribute to specific linear combination of the invariant amplitudes A_i. Helicity amplitudes are not eigenstates of parity and the $t-$channel parity conserving helicity amplitudes (PCHAs) correspond to linear combination, [11, 12]

$$\hat{T}^{\eta}_{\lambda'\lambda} = \frac{1}{\sqrt{2}} \left(\hat{T}_{\lambda'\lambda} + \eta(-1)^{\lambda'} \hat{T}_{\lambda'-\lambda} \right). \quad (4)$$

where η is the t-channel naturality, $i.e.$ $\eta = P(-)^J$ where P is the intrinsic parity and J is the spin of the exchange Reggeon in the $t-$channel. As shown in the Appendix A, the relations between PCHAs and invariant amplitudes are [13]

$$\hat{T}^+_{01} = -2k_t\sqrt{t}(-A_1 + 2MA_4) \quad (5a)$$

$$\hat{T}^-_{01} = -4p_t k_t(A_1 + tA_2) \quad (5b)$$

$$\hat{T}^+_{11} = -2k_t(2MA_1 - tA_4) \quad (5c)$$

$$\hat{T}^-_{11} = \ \ 4p_t k_t\sqrt{t}A_3 \quad (5d)$$

with M being the nucleon mass. The photon momentum, k_t and the proton momentum p_t evaluated in the $t-$channel $cf.$ Eq. (A4), contain the remaining kinematical singularities in t. We can now define four amplitudes, free of kinematical singularities that have well defined quantum numbers (η and CP) in the $t-$channel. These are,

$$F_1 = -A_1 + 2MA_4, \quad \eta = +1, \quad CP = +1, \quad (6a)$$

$$F_2 = A_1 + tA_2, \quad \eta = -1, \quad CP = -1, \quad (6b)$$

$$F_3 = 2MA_1 - tA_4, \quad \eta = +1, \quad CP = +1, \quad (6c)$$

$$F_4 = A_3, \quad \eta = -1, \quad CP = +1. \quad (6d)$$

Only negative charge conjugation, $C = -1$ exchanges, couple to $\gamma\pi^0$. For positive naturality, these correspond to vector trajectories ω ($I^G = 0^-$) and ρ ($I^G = 1^+$) and contribute to F_1 and F_3. For negative η the axial-vector trajectories h ($I^G = 0^-$) and b ($I^G = 1^+$) contribute to F_2. There are no known mesons contributing to F_4. The lowest mesons in the $t-$channel contributing to F_4 would be the ρ_2 and ω_2 with $J^{PC} = 2^{--}$. Therefore in the following we ignore the F_4 (although there are some indications that F_4 might not be exactly zero [14]).

Using the invariant amplitudes F_i defined in Eq. (6) one can compute all observables. In particular we are interested in the differential cross section and the single polarization asymmetries. [15]. The beam asymmetry is $\Sigma = (d\sigma_\perp - d\sigma_\parallel)/(d\sigma_\perp + d\sigma_\parallel)$ where $d\sigma_\perp$ $(d\sigma_\parallel)$ is the differential cross section with photon polarization along the x (y) axis and the z axis along the direction of the photon momentum and y perpendicular to the reaction plane. The target (recoil) asymmetry is defined as $T(R) = (d\sigma_\uparrow - d\sigma_\downarrow)/(d\sigma_\uparrow + d\sigma_\downarrow)$ and measures the asymmetry of the spin polarization of the target (recoil) nucleon.

At high energies, keeping only the leading s dependence in the kinematical factors relating the differential

cross section to the scattering amplitude, one finds [14][1]

$$\frac{d\sigma}{dt} \approx \frac{1}{32\pi} \left[\frac{|F_3|^2 - t|F_1|^2}{4M^2 - t} + |F_2|^2 - t|F_4|^2 \right] \quad (7a)$$

$$\Sigma\frac{d\sigma}{dt} \approx \frac{1}{32\pi} \left[\frac{|F_3|^2 - t|F_1|^2}{4M^2 - t} - |F_2|^2 + t|F_4|^2 \right] \quad (7b)$$

$$T\frac{d\sigma}{dt} \approx \frac{1}{16\pi} \sqrt{-t} \, \text{Im} \left[\frac{F_3 F_1^*}{4M^2 - t} + F_4 F_2^* \right] \quad (7c)$$

$$R\frac{d\sigma}{dt} \approx \frac{1}{16\pi} \sqrt{-t} \, \text{Im} \left[\frac{F_3 F_1^*}{4M^2 - t} - F_4 F_2^* \right]. \quad (7d)$$

The differential cross section in physical units (μb GeV^{-2}) is obtained by multiplying the right hand sides by the conversion factor $1 = 389.4 \, \mu$b GeV^2. These asymptotic formulas are useful for identifying contributions from the individual Regge contributions to the amplitudes F_i. In numerical calculations that follow, for the differential cross section, we use the complete expression

$$\frac{d\sigma}{dt} = \frac{1}{64\pi} \frac{|k_t|^2}{4M^2 E_\gamma^2} \Big[\ 2|\sin\theta_t|^2 \left(|2p_t F_2|^2 - t|F_1|^2 \right)$$
$$+ (1 - \cos\theta_t)^2 \left| F_3 + 2\sqrt{t}p_t F_4 \right|^2$$
$$+ (1 + \cos\theta_t)^2 \left| F_3 - 2\sqrt{t}p_t F_4 \right|^2 \Big], \quad (8)$$

where E_γ is the beam energy in the laboratory frame. To check the validity of the asymptotic approximation, in Section V we compare the results obtained using Eq. (7) and Eq. (8). In calculations of the spin asymmetries, however, we use the asymptotic formulas of Eq. (7) since the finite-s corrections cancel in the ratio of cross sections.

Most of the available data comes from the proton target with only a few measurements of the differential cross sections on the neutron. The corresponding amplitudes are related by isospin symmetry. In the t-channel, the isospin decomposition for each of the four invariant amplitudes is is given by [10]

$$A_{\alpha\beta}^a = A^{(+)}\delta^{a3}\delta_{\alpha\beta} + A^{(-)}\frac{1}{2}[\tau^a, \tau^3]_{\alpha\beta} + A^{(0)}\tau_{\alpha\beta}^a. \quad (9)$$

with $A^{(+)}$, $A^{(-)}$ and $A^{(0)}$ corresponding to t-channel isospin $I^G = 0^-$, 1^- and 1^+ and a, α, β being the isospin indices for the pion, the two nucleons, respectively. Only $A^{(+)}$ and $A^{(0)}$ contribute to π^0 photoproduction. We note that the isovector exchange contribution contributes with opposite sign to proton and neutron amplitudes, *i.e.*

$$A(\gamma p \to \pi^0 p) = A^{(+)} + A^{(0)}, \quad (10a)$$
$$A(\gamma n \to \pi^0 n) = A^{(+)} - A^{(0)}. \quad (10b)$$

———————

[1] We corrected the sign of F_1 in the target and recoil asymmetries, *cf.* Appendix B.

III. THE REGGE MODEL

In this section we specify the model for the t-channel kinematical singularity free amplitudes $F_i(s,t)$. The contribution of a Regge pole, $R(s,t)$ and a Regge-Pomeron cut $R_c(s,t)$ to $F_i(s,t)$ have asymptotic energy dependence determined by the Regge trajectory $\alpha(t)$[1, 11, 16]. The residues are analytical in t in the s-channel physical region and have zeros that are forced by spin considerations. In particular, in the physical region of the t-channel, net helicity in ether, the $\gamma\pi^0$ or the $N\bar{N}$ vertex cannot exceed $J = \alpha(t)$ for non-negative, integer values of J. In addition, in the s-channel physical region the amplitude cannot have singularities other then threshold branch points. A simple model that builds in these constraints is given by,

$$R(s,t) = \frac{\pi}{\Gamma(\alpha(t))} \frac{1 - e^{-i\pi\alpha(t)}}{2\sin\pi\alpha(t)} \left(\frac{s}{s_0}\right)^{\alpha(t)-1}, \quad (11)$$

$$R_c(s,t) = \frac{1}{\log(s/s_0)} \frac{\pi}{\Gamma(\alpha(t))} \frac{1 - e^{-i\pi\alpha(t)}}{2\sin\pi\alpha(t)} \left(\frac{s}{s_0}\right)^{\alpha(t)-1}. \quad (12)$$

The energy dependence yields the expectation $d\sigma/dt \propto s^{\alpha(t)}$ once the extra energy power coming from the half-angle factor in Eq. (2) is included. These expressions can in principle be multiplied by an analytical function of t, that can be, for example fixed by the data. To minimize the number of parameters in the model, we will attempt to fit the data with minimal such modifications (see below) observing that the scale s_0 already leads to an exponential fall off with t for $s > s_0 = 1$ GeV^2 which is typical. For positive values of spin, $J = \alpha > 0$, the signature factor $1 - e^{i\pi\alpha}$ is finite for the right exchanges, *i.e.* odd-spin mesons lying on the vector or axial-vector trajectories and it vanishes, canceling the zero of $\sin\pi\alpha$ for the wrong spin exchanges *i.e.* even-spin mesons. For negative odd-values of α there would be unphysical poles. The Γ function in the denominator is introduced to remove these poles from the s-channel physical region. It also leads to zeros of the amplitude at non-positive even integer values of α. As discussed above Eq. (11) $\alpha = 0$ is indeed forbidden by spin considerations since it is less then the magnitude of net helicity in the $\gamma\pi^0$ vertex. In principle there is no need for the amplitude to vanish at negative even-integer values of α. Thus the particular choice of using the Γ function to cancel the unphysical poles of the so-called Regge propagator, $1/\sin\pi\alpha$, has to be confronted with the data and can in principle be modified if needed. We will further explore the consequences of this choice in Section IV and V.

For values of α which are not too far from positive integers Regge pole amplitudes are similar to this of particle exchange. We therefore use a one-particle-exchange model for a vector and axial-vector meson to impose further constraints. The t-channel amplitude for a vector

meson exchange, *e.g.* $V = \rho, \omega$ is given by (*cf.* Appendix A)

$$\frac{i\varepsilon_{\alpha\beta\mu\nu}k^\mu\epsilon^\nu q^\alpha}{t - m_V^2}\bar{u}_4\left[g_4^V\gamma^\beta + g_1^V\gamma^{[\beta}\gamma^{\sigma]}(p_2 - p_4)_\sigma\right]v_2$$

$$= \bar{u}_4\left[\frac{g_4^V M_4 + g_1^V(tM_1 - M_2)}{t - m_V^2}\right]v_2, \quad (13)$$

where $\bar{u}_4 \equiv \bar{u}(p_4, \mu_4)$ and $v_2 \equiv v(-p_2, \mu_2)$ with the right hand side written in terms of the CGLN basis tensors M_i. Similarly for the axial vectors, $A = b, h$ one finds,

$$g_2^A\epsilon^\mu\left[k \cdot q g_{\mu\alpha} - q_\mu k_\alpha\right]\frac{\bar{u}_4\gamma_5 p^\alpha v_2}{t - m_A^2} = \frac{\bar{u}_4 g_2^A M_2 v_2}{t - m_A^2}. \quad (14)$$

Comparing with Eq. (1) on concludes that, for the vector contribution, $A_1 \propto g_1 t, A_2 \propto -g_1$ and $A_4 \propto g_4$. We also note that in the s-channel frame g_4 corresponds to helicity non-flip coupling and g_1 to helicity flip coupling. Near the pole, the tree-level propagator $1/(t - m_V^2)$, corresponds to $1/\sin\pi\alpha$. We also note that, as expected, the vector exchanges contribute only to F_1 and F_3. Also, as expected we find that the axial vector change contributes only to F_2 via $A_2 \propto g_2^A$.

The data, as it will be described in the next section, indicate that corrections to the Regge pole approximation are needed. We then anticipate and add in our model the cut associated with the vector trajectory. Their role will be clarified by comparing to the data. The $t-$dependence of Regge-Pomeron cut residues is, *a priori*, different from that of the Regge poles. For simplicity, however, we will use the same $t-$dependence as for the corresponding pole. Taking these considerations into account leads to the following expressions for the invariant amplitudes F_i

$$F_1 = (-g_1 t + 2Mg_4)R^V + (-g_1^c t + 2Mg_4^c)R_c^V(s,t)),$$
$$F_2 = g_2 t R^A,$$
$$F_3 = (2Mg_1 - g_4)t R^V + (2Mg_1^c - g_4^c)t R_c^V(\alpha_c),$$
$$F_4 = 0. \quad (15)$$

We do not include cut contributions in the axial exchange amplitudes. In Eqs (15), $(g_1, g_2, g_4, g_1^c, g_4^c)$ are real parameters to be determined by fitting the data. Because of the connection with the one-particle exchange model they can be related to the products of $\gamma\pi^0$ and NN couplings of vectors and axial vectors [17]. Since matching between particle exchange and Regge amplitudes is only exact at the t-channel pole, the polynomial t dependence in Eqs (15) is rather arbitrary, we keep it nevertheless to allow for more flexibility in describing the t-dependence.

The subscripts V and A in Eq. (15) specify the Regge trajectory $\alpha = \alpha_V(t)$ or $\alpha = \alpha_A(t)$ to be used in the Regge amplitudes of Eq. (11). We assume exchange degeneracy *i.e.* the same trajectory α_V for ω and ρ, and the same axial trajectory, α_A for b and h which, including the cut, we take to be linear,

$$\alpha_V(t) = \alpha_{V0} + \alpha_V' t, \qquad \alpha_A(t) = \alpha_{A0} + \alpha_A' t,$$
$$\alpha_c(t) = \alpha_{c0} + \alpha_c' t. \quad (16)$$

Furthermore, from Eq. (10) it follows that for the $g_1 = \pm g_1^\rho + g_1^\omega$, $g_4 = \pm g_4^\rho + g_4^\omega$ and $g_2 = \pm g_2^b + g_2^h$ with the upper/lower sign referring the proton/neutron amplitudes, respectively. In addition to the five couplings we need to determine the six trajectory parameters $(\alpha_{V0}, \alpha_V', \alpha_{A0}, \alpha_A', \alpha_{c0}, \alpha_c')$. Trajectory parameters are constrained by the meson mass-spin relations and are expected to be approximately given by [1]

$$\alpha_V(t) = 1 + 0.9(t - m_\rho^2) \qquad \sim 0.5 + 0.9t \quad (17a)$$
$$\alpha_A(t) = 1 + 0.7(t - m_{b_1}^2) \qquad \sim 0.7t \quad (17b)$$

In a simple model for Pomeron exchange [1], the Regge-Pomeron cut trajectory has an intercept, $\alpha_{c0} = \alpha_{V0}$ and a slope close to that of the Pomeron, *i.e* we expect the cut trajectory to approximately give by

$$\alpha_c(t) \sim 0.5 + 0.2t. \quad (18)$$

IV. RESULTS

A. Data selection and interpretation

The $t-$channel exchanges govern in the physics of the $s-$channel region only for large energies and small momentum transfers. The exact region of validity of Regge theory will be deduced by analyzing the data. In the region $E_\gamma \geq 2$ GeV and $|t| < 3$ GeV^2 there are data on differential cross sections [18–21] shown in Fig. 1, the beam asymmetry [18], shown in Fig. 2, the ratio of differential cross section on neutron to proton targets, shown in Fig. 2, and on target and recoil asymmetries [22–24], shown in Fig. 4.

The differential cross section in the energy range $E_\gamma = 6-15$ GeV has a dip at $t \sim -0.5$ GeV^2. This value of momentum transfer is close to the wrong signature point of the vector trajectory *i.e.* $\alpha_V(t) = 0$. As explained in the previous section, vector exchange is expected to vanish at $\alpha_V = 0$ since it corresponds to a nonsense point, *i.e.* unphysical helicity coupling. The minimum seen in the data has therefore a clear interpretation within the Regge theory, however, a single Regge pole model would imply vanishing of the cross section at the non-sense point which is inconsistent with the data. The disappearance of the dip at lower energies, $E_\gamma \lesssim 2$ GeV can be used as signal for inapplicability of the simple Regge model. The data in the intermediate region $E_\gamma = 2 - 6$ GeV, however, does not give a precise determination of the energy where the simple Regge picture breaks down.

The beam asymmetry is sensitive to exchange on trajectories corresponding to mesons with negative naturality, since it is given by

$$\Sigma = \frac{|\omega + \rho|^2 - |h + b|^2}{|\omega + \rho|^2 + |h + b|^2} \quad (19)$$

where each term corresponds to a single Regge amplitude. With the vector contribution being close to zero
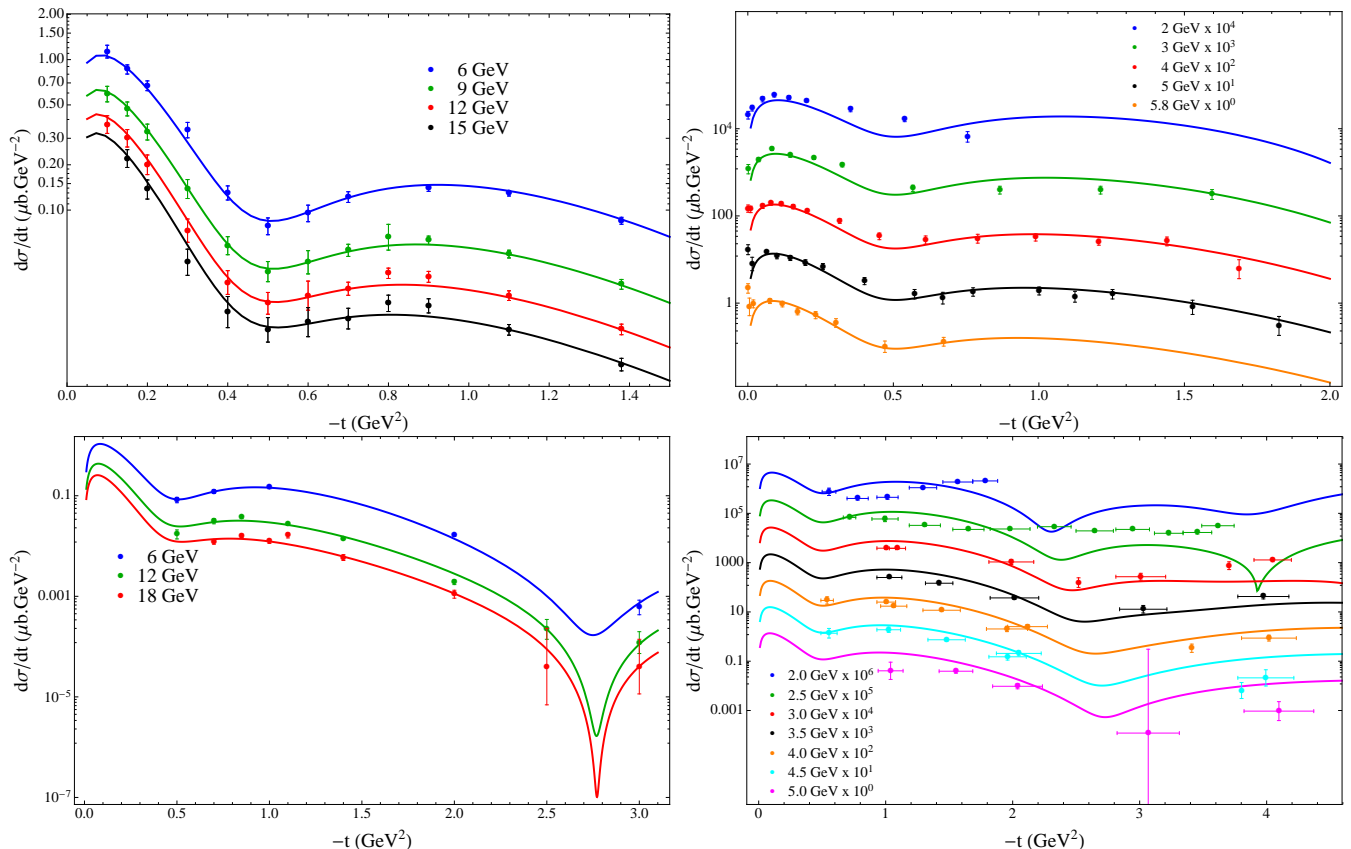
FIG. 1. (Color online). Differential cross section. Only the data in the region $E_\gamma \geq 4$ GeV and $|t| \leq 3$ GeV^2 are used in the fit, see text. Data from [18–21, 25]

at $t \sim -0.5$ GeV^2, the beam asymmetry is predated to be $\Sigma \sim -1$. In the other limit, with the axial vector being close to zero, $\Sigma = +1$ and deviations from this value measures the strength of the axial vector Regge trajectory contributions, as seen in Fig. 2. For not too large momentum transfers, $|t| < 2.5$ GeV^2, that value of α for the vector trajectory is larger than for the axial, $\alpha_V(t) > \alpha_A(t)$, *cf.* Eq. (17), thus as energy increases, the contribution of axial exchanges relative to vector exchanges decreases. The beam asymmetry is therefore expected to approach one as the energy increases. The data in Fig. 2, however, shows an approximatively constant beam asymmetry as a function of energy.

The ratio of the differential cross sections on the neutron compared to the proton target also indicates presence of exchanges other than single Regge poles. This ratio is given by

$$\frac{d\sigma(n)/dt}{d\sigma(p)/dt} = \frac{|\omega - \rho|^2 + |h - b|^2}{|\omega + \rho|^2 + |h + b|^2}. \quad (20)$$

Since, phenomenologically it is observed that the isoscalar exchanges ω and h have trajectory slopes approximatively equal to those of their vector partners, ρ and b, the ratio is expected to be relatively energy independent. The data shown in the right panel in Fig. 2 indicates a significant deviations from this expectation.

We conclude that qualitative features of the data are consistent with the single Regge pole approximations, however, quantitative description requires inclusion of other contributions, *e.g.* daughter trajectories or cuts.

B. Cut versus daughter

As discussed above, near the nonsense point $\alpha = 0$ ($t \sim -0.5$ GeV^2), differential cross section is small but non-vanishing. Zero in the vector Regge exchange amplitude can be lifted by either axial Regge poles or corrections to the single Regge pole model. In order to determine which contribution dominates over the vector exchange we compare energy dependence of the differential cross section at $t = -0.5$ GeV^2 to that at $t = -0.1$ GeV^2, where the vector pole is expected to dominate. For the axial or daughter trajectory this ratio would decrease with energy since both have an intercept which is smaller than that of the vector trajectory. On the other hand, if it is a Regge-Pomeron cut the ratio would, up to logarithmic corrections, be approximatively energy independent since the intercept of the cut is similar to that of the pole, *cf.* Eq. (11). The measured ratio between differential cross sections at these two values of momentum transfer is 6.9%, 6.6% and 6.5% at $E_\gamma = 6$, 9 and 12
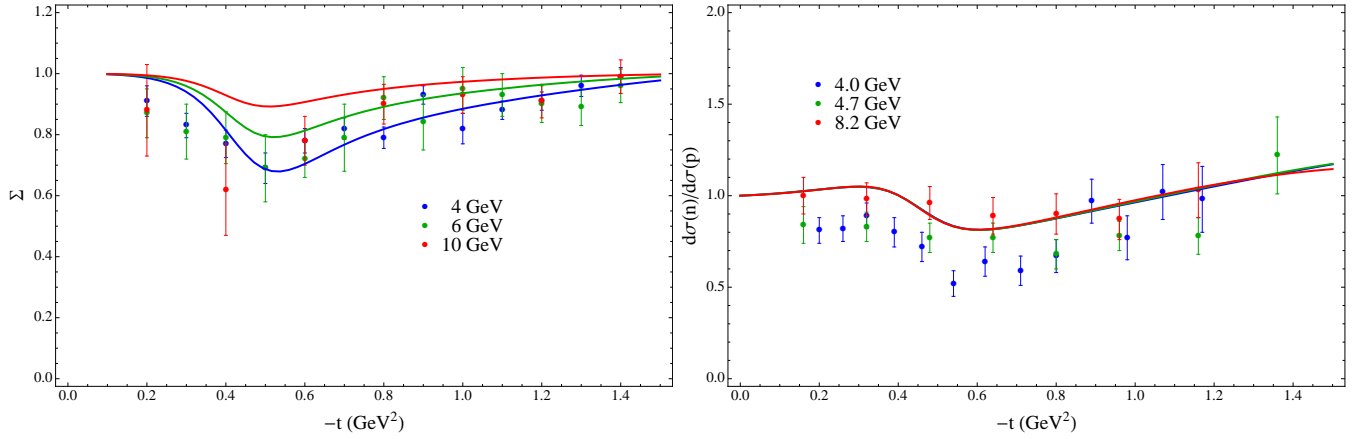
FIG. 2. (Color online). Beam asymmetry (left) and ratio of differential cross sections with neutron target to proton target (right). Data from [18] (left) and [21, 25] (right)

GeV, respectively. This is almost energy independent and we conclude that cuts might be more relevant than sub-leading Regge poles in filling up the zero at $t \sim -0.5$ GeV^2. Another discriminator between cuts and poles is the t-dependence. The logarithmic slope shown in Fig. 1, in the region $t \in [-0.1, -0.4]$ GeV^2 where the pole dominates is larger than that in the region $t \in [-0.9, -1.4]$ GeV^2. Since cut has a smaller slope than a pole we conclude that at the larger value of $|t|$ where the leading pole is suppressed it is the cut that dominated the differential cross section. To illustrate the difference between the vector-Regge-Pomeron cut model and a model with a sub-leading pole we compare their predictions for the differential cross section. In π^0 photoproduction, as shown later, the dominant Regge-pole contribution comes from the ω exchange, which is predominantly helicity-non-flip at the nucleon vertex in the s-channel. We thus place the ω contribution into the A_4 amplitude and take,

$$F_1 = 2Mg_4^p R(\alpha_V) + 2Mg_4^c R(\alpha_c) \qquad (21a)$$

$$F_3 = -tg_4^p R(\alpha_V) - tg_4^c R(\alpha_c) \qquad (21b)$$

with $g_4^p = 1$ and $g_4^c = 0.1$, representing a 10% contribution of the ω-Pomeron cut at the amplitude level. For a model with a daughter trajectory, we take

$$F_1 = 2Mg_4^p R(\alpha_V) + 2Mg_4^d R(\alpha_d) \qquad (22a)$$

$$F_3 = -tg_4^p R(\alpha_V) - tg_4^d R(\alpha_d) \qquad (22b)$$

with $g_4^p = 1$ and $g_4^d = 0.5$. The couplings were chosen so that both models yield comparable cross sections.

The predicted deferential cross section for the two models at two photon energies $E_\gamma = 3$ and 9 GeV is shown in Fig. 3. As expected, the logarithmic slope in the range 1 GeV$^2 < |t| < 2$ GeV^2 is different in the two models, the cut resulting in a smaller slope and dominating in this region of momentum transfer. Both models, have the first minimum coinciding with zero of the ω Regge pole but the energy dependence of the zero is
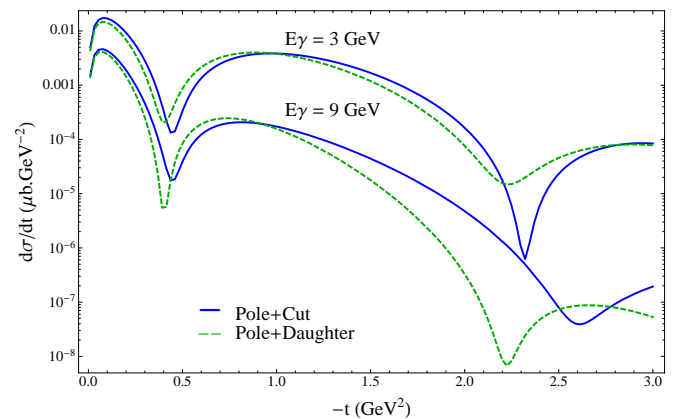

FIG. 3. (Color online). The two simple models discussed in the text for a beam energy of 3 and 9 GeV.

deferent. Specifically, the ratio between the first maximum, at around $t = -0.1$ GeV^2 and the first minimum, at around $t = -0.4$ GeV^2 is almost energy independent for the model with the cut. The weak energy dependence of the dip and the smaller logarithmic slope at larger momentum transfers of the model with the cut make it phenomenologically more appealing compared to the model with an additional pole.

We also note, that in the model with the cut, the position of the second dip, around $|t| \sim 2.2 - 2.6$ GeV^2 seems to move with energy more than in the model with a second pole. With the existing data it is not possible to test this prediction, however, it might be possible with the forthcoming CLAS data [3].

C. Fitting procedure

The parameters of the Regge model from Sec. III are determined as follows. First we fix the vector Regge pole and the associated Regge cut parameters by fitting the

differential cross section of photoproduction on the proton target. This does not determine the isospin of the vector exchange. The axial vector pole contribution to the differential cross section is small, (cf. Sec. IV B) and in the fit to the cross section it is ignored. The axial vetoer Regge pole parameters are determined by fitting the beam asymmetry, once the vector exchanges are fixed by the differential cross section. The target and recoil asymmetries are not included in the fits and constitute a prediction of the model.

We include in the fit the data from [18] and [19] in the kinematical range $E_\gamma \geq 6$ GeV and $|t| \leq 3$ GeV^2. We also include data from [21] for $E_\gamma \geq 4$ GeV and $0.01 < |t| \leq 3$ (in GeV^2). We exclude the region $|t| < 0.01$ GeV^2 since it is dominated by the Primakoff process. We do not include the data from [20], which is compatible with the other data, but has much wider t-bins and no data points close to the forward direction. We have found that the lower energy data $E_\gamma < 4$ GeV from [21] results in a significantly larger $\chi^2/$d.o.f. > 2 compared to the other sets. Therefore we fix the model parameters in data above 4 GeV and predict the cross section in the lower energy range $E_\gamma < 4$ GeV. For $E_\gamma \geq 4$ GeV the model reproduces the data in the whole range of $|t| \leq 3$ GeV^2. Overall the fit results in $\chi^2/$d.o.f. $= 1.75$ and for the parameters of the vector pole and cut are find (with α' is in GeV^{-2})

$$g_1 = \quad 3.89 \pm 1.68 \text{ GeV}^{-4}, \quad \alpha_{V0} = 0.44 \pm 0.01 \quad (23a)$$
$$g_4 = -10.14 \pm 0.65 \text{ GeV}^{-3}, \quad \alpha'_V = 1.10 \pm 0.05 \quad (23b)$$
$$g_1^c = \quad -1.76 \pm 0.39 \text{ GeV}^{-2}, \quad \alpha_{c0} = 0.46 \pm 0.04 \quad (23c)$$
$$g_4^c = \quad -3.58 \pm 0.93 \text{ GeV}^{-4}, \quad \alpha'_c = 0.17 \pm 0.01. \quad (23d)$$

Although we did not constrain parameters of the trajectories, the fit finds the vector trajectory consent with expectations, cf. Eq. (17).

With the vector Regge pole and cut parameters determined using the high-energy data, in Fig. 1 we compare model prediction with the data in the lower-energy region, $E_\gamma \geq 2$ GeV. It appears that the simple Regge pole plus cut model is qualitatively consistent with the data in this region, although the data in this region is rather sparse and it is impossible to clearly identify the region of applicability of the Regge theory.

As discussed in Sec. IV A, we assume that the main contribution to beam asymmetry comes form the axial vector Regge poles. From a fit to the beam asymmetry in the energy range $4 \leq E_\gamma(\text{GeV}) \leq 10$ with the vector Regge exchanges fixed by Eq. (23) we find

$$g_2 = -8.89 \pm 2.30 \text{ GeV}^{-4}, \quad (24a)$$
$$\alpha_{A0} = -0.19 \pm 0.30 \quad (24b)$$
$$\alpha'_A = \quad 1.02 \pm 0.18 \text{ GeV}^{-2}. \quad (24c)$$

with $\chi^2/d.o.f = 1.73$. The large uncertainty obtained for the intercept is not surprising. It originates from the discrepancy in the energy dependence between the data and the model with a a single axial pole cf. Sec. IV A.

Since the differential cross section and the beam asymmetry do not discriminate between isovector and isoscalar Regge poles the coupling parameters in Eq. (23) are the sum of the two exchanges. The helicity flip and non-flip residues in the $s-$channel are proportional to g_1 and g_4 respectively. If we assume that in the $s-$channel ω trajectory is dominantly helicity non-flip so that, $g_4^{(c)} = g_4^{(c)\omega}$, the ρ trajectory helicity flip, i.e. $g_1^{(c)} = g_1^{(c)\rho}$ [1], and we neglect the h trajectory, i.e. $g_2 = g_2^b$, we can make a prediction for the ratio of the differential cross section on the neutron and proton targets. The two are related by a sign change in g_1, g_1^c and g_2 cf. Eq. (10). We compare this prediction with the data [21, 25] in the energy range $4 \leq E_\gamma(\text{GeV}) \leq 8.2$ in Fig. 2. The angular distribution of the data is well reproduced by our theoretical prediction. However, as we already commented in Sec. IV A, the energy dependence of our model is only qualitatively consistent with the data. The degeneracy between ω and ρ trajectories produced a ratio of the differential cross section on the neutron and proton targets independent of the energy.

The target [22, 23] and recoil asymmetries [24] are compared to the data in Fig. 4. The data is given in the energy range from $E_\gamma = 4.1$ GeV to $E_\gamma = 6.3$ GeV and we compare with model predictions at $E_\gamma = 4, 5$ and 6 GeV. The target and recoil asymmetries are compatible with each other indicating that amplitude F_4 is small cf. Eq. (7). Since we have set $F_4 = 0$ the target and recoil asymmetries in Eq. (7) are equal and proportional to Im $F_3 F_1^*$. Non-vanishing imaginary part requires at least two amplitudes are present, e.g. a pole and a cut. Since the vector exchange produces a zero at the nonsense point $\alpha = 0$ our model predicts that both asymmetries change sign at $t = -0.4$ GeV^2, which is qualitatively consistent with the data.

We conclude this section with comparison, shown in Fig. 5, of the differential cross section computed using the exact expression and the high-energy approximation given by Eq. (8) and Eq. (7), respectively. We observe that the high-energy limit is a good approximation even at the lowest energies considered in the fits. The discrepancy increases as $|t|$ grows, for example, at $E_\gamma = 6$ GeV, and $t = -1$ GeV^2 the difference is approximately 12%.

V. PREDICTIONS

We give predictions of the model at various beam energies in Fig. 6. The energy range $E_\gamma = 3 - 6$ GeV corresponds to the recent CLAS measurement [3]. We also give a prediction for higher energy $E_\gamma = 9$ GeV relevant for the forthcoming measurements at GlueX. We show the differential cross section both as a function of momentum transfer and the s-channel scattering angle in the range $|t| < 3$ GeV^2. In the description of the model we repeatedly emphasized the role of zeros in Regge pole residues, cf. Eq. (11). These correspond to nonsense points, with α equal to non-positive integer. The first
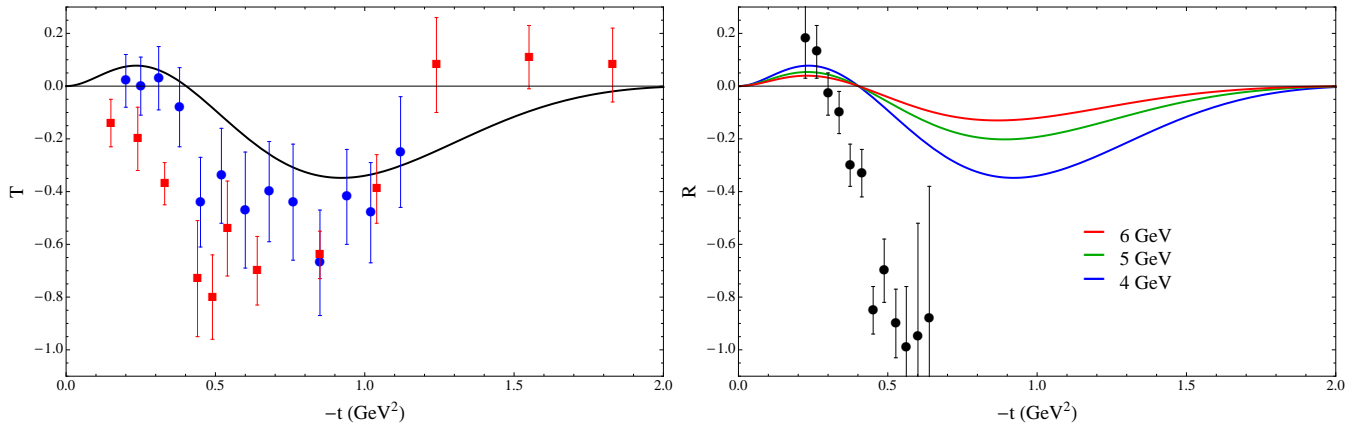
FIG. 4. Color online. Target asymmetries at $E_\gamma = 4$ GeV from [22, 23] (left) and recoil (right) asymmetries. Data from (target asymmetry) and from [24] (recoil asymmetry).
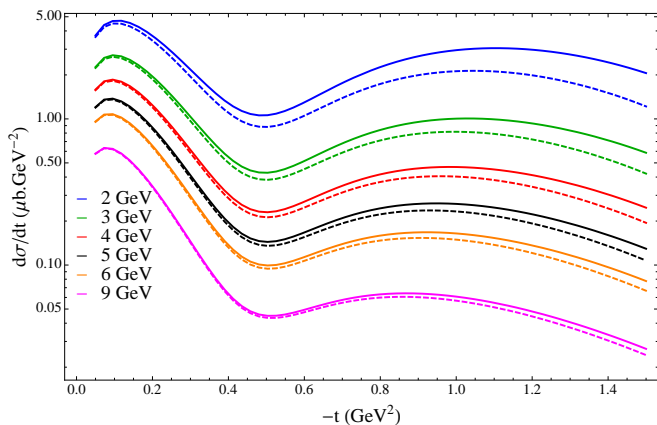

FIG. 5. Color online. Comparison of differential cross section between the high energy limit Eq. (7) (solid lines) and the full expression Eq. (8) (dashed lines) for a wide range in incident beam energies.

zero appears in the vector trajectory, at $\alpha_V = 0$, and is well established empirically, seen as a dip in the differential cross section at $t \sim -0.5$ GeV^2. At larger $|t|$, zeros corresponding to lower integer values of Regge trajectories should become visible. For the vector trajectory, $\alpha_V(t) = -2$ corresponds to $t \sim -2.2$ GeV^2 and zero of the cut, $\alpha_c(t) = 0$ arises at $t \sim -2.8$ GeV^2. We therefore expect the differential cross section to dip in this region of momentum transfer. Indeed for energies below $E_\gamma = 6$ GeV, the dip appears, *cf.* Fig. 6, and is energy dependent, which would be expected from the interference of the pole and the cut amplitude. There are however only a few data points at large $|t|$ to make a detailed comparison wit the model. The second minimum in the differential cross section can therefore be used to discriminate between various models for the subleading Regge contributions interfering with the dominant vector pole. In the energy range $E_\gamma = 4 - 5.5$ GeV, the second dip should arise at angle $\theta \sim 60° - 80°$, and should be visible in the

CLAS data [3].

VI. CONCLUSION

We investigated photoproduction of neutral pions for energies above s-channel resonance region. Our amplitudes include the leading Regge poles in the t-channel and describe well the differential cross section for beam energies above 4 GeV and for momentum transferred squared above -3 GeV^2. The first dip seen at $t \sim -0.5$ GeV^2, is characteristic to the vector Regge pole and seems to persist down to $E_\gamma = 3$ GeV although the quantitative analysis is not possible given the quality of the data in the intermediate energy region $3 - 4$ GeV. Below $E_\gamma = 3$ GeV nucleon resonances become visible and were the focus of most of the recent efforts in pion photo production [5–8]. These studies could benefit from the results of the higher energy data analysis, for example by implementing finite-t or finite energy sum rule constraints on the resonance models. The resulting baryon spectrum from the analysis in Refs [7, 8] is compared in Ref. [26]. A common agreement is found for the lowest nucleon excitations, but both spectra strongly disagree in the center-of-mass energies $1.7 - 2.0$ GeV. We hope that our amplitudes will provide significant insights in the baryon spectrum to solve the remaining ambiguities in this topic. The sum rules for pion photoproduction were studied in the past [4], however, only now precise partial waves for the low energy data are available.

In Sec. IV A we analyzed the energy dependence of the beam asymmetry for the reaction $\gamma p \to \pi^0 p$ and the differential cross section for the reaction $\gamma n \to \pi^0 n$. Based on the expected trajectories for the ω, ρ and the b poles and the dominance of these Regge poles, we concluded that the beam asymmetry should approach one as the energy increases and the differential cross section for $\gamma n \to \pi^0 n$ should have the same energy dependence as for the reaction $\gamma p \to \pi^0 p$. Both are only qualitatively reproduced, however, the data for these observables at
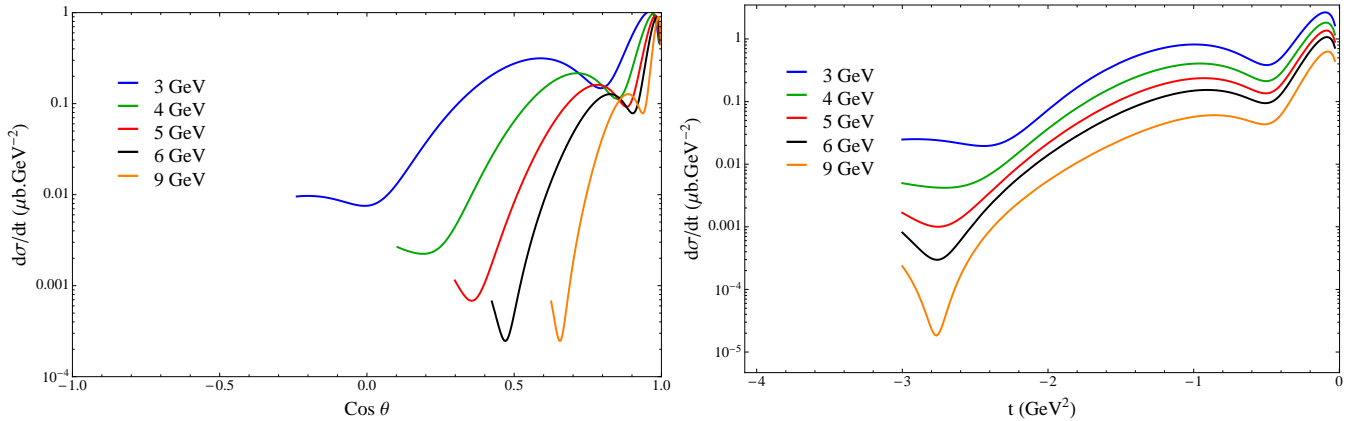
FIG. 6. Model prediction for the differential cross section at CLAS and GlueX energies.

high energies is rather sparse and we hope that more precise data, including the forthcoming data from CLAS will help clarifying these issues.

All the material, including data and software are available in an interactive from online. We invite the interested readers to contact the authors.

Appendix A: $t-$channel helicity amplitudes

In this Appendix we compute the combinations of scalar amplitudes with good quantum numbers of the $t-$channel $\gamma(k)\pi^0(-q) \rightarrow \bar{N}(-p_2)N(p_4)$. The Mandelstam variables $s = (k + p_2)^2$, $t = (k - q)^2$, $u = (k - p_4)^2$ are related through $s + t + u = 2M^2 + \mu^2$. In the $t-$channel, the physical domain of the Mandelstam variable is ($t \geq 4M^2, s \leq 0$).

We start by decomposing the $t-$channel helicity amplitudes in the tensor basis [10].

$$A^t_{\lambda_4\lambda_2,\lambda_1}(s,t) = \bar{u}_{\lambda_4}(p_4) \sum_{i=1}^{4} A_i(s,t) M_i v_{\lambda_2}(-p_2). \quad (A1)$$

where A_i are sclaar function and

$$M_1 = \frac{1}{2}\gamma_5\gamma_\mu\gamma_\nu F^{\mu\nu}, \quad (A2a)$$

$$M_2 = 2\gamma_5 q_\mu p_\nu F^{\mu\nu}, \quad (A2b)$$

$$M_3 = \gamma_5 q_\mu\gamma_\nu F^{\mu\nu}, \quad (A2c)$$

$$M_4 = \frac{i}{2}\varepsilon_{\alpha\beta\mu\nu}\gamma^\alpha q^\beta F^{\mu\nu}, \quad (A2d)$$

with $p = (p_2 + p_4)/2$. The tensors $F^{\mu\nu} = \epsilon^\mu(k,\lambda_1)k^\nu - k^\mu\epsilon^\nu(k,\lambda_1)$ satisfy gauge invariance by construction.

In the $t-$channel center of mass frame,

$$k^\mu = (k_t, 0, 0, k_t), \quad p_2^\mu = (-E_N^t, -p_t\sin\theta_t, 0, -p_t\cos\theta_t),$$
$$q^\mu = (E_\pi^t, 0, 0, k_t), \quad p_4^\mu = (+E_N^t, -p_t\sin\theta_t, 0, -p_t\cos\theta_t). \quad (A3)$$

The first component is the energy and the metric is diag$(+,-,-,-)$. E_N^t and E_π^t are the nucleon and pion energies. The scattering angle in the $t-$channel is θ_t. p_t is the momentum of the nuclei in their rest frame. In this frame, k_t is the photon and pion momenta. The masses of the pion and the nucleon are respectively μ and M. The kinematical quantities are

$$E_\pi^t = (t + \mu^2)/2\sqrt{t} \qquad E_N^t = \sqrt{t}/2 \quad (A4a)$$

$$p_t = \sqrt{t/4 - M^2} \qquad k_t = (t - \mu^2)/2\sqrt{t} \quad (A4b)$$

$$\cos\theta_t = \frac{s - u}{4k_tp_t} \qquad \sin\theta_t = \frac{\sqrt{\phi/t}}{2k_tp_t}, \quad (A4c)$$

with $\phi = stu - \mu^2 M^2(\mu^2 - t) - tM^4 > 0$. In the s-channel physical region we use the convention of Trueman and Wick Ref [27], and evaluate the square root with the prescription $s \rightarrow s + i\epsilon$ and $t \rightarrow t - i\epsilon$. It is useful to remember that, in the $s-$channel, E_N^t, k_t and p_t are purely imaginary with a negative imaginary part, $\cos\theta_t$ is real and negative and $\sin\theta_t$ is imaginary with a positive imaginary part.

For the spinors, we use the Dirac representation. The

$\gamma-$matrices are, with σ_i the Pauli matrices,

$$\gamma^0 = \begin{pmatrix} 1_2 & 0 \\ 0 & -1_2 \end{pmatrix}, \quad \gamma^i = \begin{pmatrix} 0 & \sigma^i \\ -\sigma^i & 0 \end{pmatrix}, \quad \gamma^5 = \begin{pmatrix} 0 & 1_2 \\ 1_2 & 0 \end{pmatrix}. \tag{A5}$$

For the evaluation of Eq. (A1), the spinors are (with the lower-script $\pm \equiv \pm\frac{1}{2}$)

$$v_+(-p_2) = \begin{pmatrix} -\sqrt{E_N^t - M}\,\chi_2(\theta_t) \\ \sqrt{E_N^t + M}\,\chi_2(\theta_t) \end{pmatrix},$$

$$v_-(-p_2) = \begin{pmatrix} -\sqrt{E_N^t - M}\,\chi_1(\theta_t) \\ -\sqrt{E_N^t + M}\,\chi_1(\theta_t) \end{pmatrix}, \tag{A6}$$

$$\bar{u}_+(p_4) = \left(\sqrt{E_N^t + M}\,\chi_2^\dagger(\theta_t) \quad -\sqrt{E_N^t - M}\,\chi_2^\dagger(\theta_t) \right),$$

$$\bar{u}_-(p_4) = \left(\sqrt{E_N^t + M}\,\chi_1^\dagger(\theta_t) \quad \sqrt{E_N^t - M}\,\chi_1^\dagger(\theta_t) \right),$$

with

$$\chi_1(\theta) = \begin{pmatrix} \cos\theta/2 \\ \sin\theta/2 \end{pmatrix}, \quad \chi_2(\theta) = \begin{pmatrix} -\sin\theta/2 \\ \cos\theta/2 \end{pmatrix}, \tag{A7}$$

and the polarization tensor for the photon is $\epsilon^\mu(k,\pm 1) = (0, \mp 1, -i, 0)/\sqrt{2}$.

With these definition the $t-$channel amplitudes can be expressed in terms of the scalar amplitudes and the kinematical quantities,

$$A_{++,1}^t = \sqrt{2}k_t \frac{\sin\theta_t}{2} \left[\sqrt{t}\,(A_1 - 2MA_4) - 2p_t\,(A_1 + tA_2) \right]$$

$$A_{--,1}^t = \sqrt{2}k_t \frac{\sin\theta_t}{2} \left[\sqrt{t}\,(A_1 - 2MA_4) + 2p_t\,(A_1 + tA_2) \right]$$

$$A_{+-,1}^t = \sqrt{2}k_t \sin^2\frac{\theta_t}{2} \left[\; 2p_t\sqrt{t}A_3 - (2MA_1 - tA_4) \right]$$

$$A_{-+,1}^t = \sqrt{2}k_t \cos^2\frac{\theta_t}{2} \left[-2p_t\sqrt{t}A_3 - (2MA_1 - tA_4) \right] \tag{A8}$$

The amplitudes with negative photon helicity are obtained from the relations

$$A_{\pm\pm,-1}^t = A_{\mp\mp,-1}^t, \quad A_{\pm\mp,-1}^t = -A_{\mp\pm,-1}^t. \tag{A9}$$

In Eq. (A8), the invariant amplitudes A_i contain dynamical singularities. Some of the kinematical singularities in t are explicitly extracted (and arise in p_t, k_t and $\sqrt{t}$). All kinematical singularities in the variable s are encoded in the trigonometric functions. They arise from the spin of the external particles and are independent of the exchanged particle. They can be extracted easily from the partial wave decomposition in the $t-$channel

$$A_{\lambda_4\lambda_2,\lambda_1}^t(s,t) = \sum_{J=1}^{\infty} (2J+1)T_{\lambda'\lambda}^J(t)\,d_{\lambda'\lambda}^J(z_t). \tag{A10}$$

with $\lambda = \lambda_1 - \lambda_3 = \lambda_1$, $\lambda' = \lambda_2 - \lambda_4$ and $z_t = \cos\theta_t$. The Wigner rotation function $d_{\lambda'\lambda}^J(z_t) = \xi_{\lambda'\lambda}(z_t)P_{\lambda'\lambda}^J(z_t)$,

where P^J is a polynomial, has indeed a cut in the s variable. They originate from the half-angle factor

$$\xi_{\lambda'\lambda}(z_t) = \left(\frac{1 - z_t}{2} \right)^{\frac{1}{2}|\lambda'-\lambda|} \left(\frac{1 + z_t}{2} \right)^{\frac{1}{2}|\lambda'+\lambda|}. \tag{A11}$$

The partial waves $T_{\lambda'\lambda}^J$ have a well defined spin J but are not eigenstate of parity. The good parity combinations are $T_{\lambda'\lambda}^J \pm T_{\lambda'-\lambda}^J$. In order to form parity conserving amplitudes free of kinematical singularities, one first needs to remove the half-angle factor with the definition

$$A_{\lambda_4\lambda_2,\lambda_1}^t = \left[\cos\frac{\theta_t}{2} \right]^{|\lambda+\lambda'|} \left[\sin\frac{\theta_t}{2} \right]^{|\lambda-\lambda'|} \widehat{T}_{\lambda\lambda'}. \tag{A12}$$

Then $t-$channel parity conserving helicity amplitudes (PCHAs) are given by [11, 12]

$$\widehat{T}_{\lambda'\lambda}^\eta = \frac{1}{\sqrt{2}} \left(\widehat{T}_{\lambda'\lambda} + \eta(-1)^{\lambda'}\,\widehat{T}_{\lambda'-\lambda} \right). \tag{A13}$$

η is called the naturality as it corresponds to $P(-)^J$ for an exchanged particle of parity P and spin J in the $t-$channel. Using the expressions (A8), we obtain the relations between the PCHAs and the invariant amplitudes

$$\widehat{T}_{01}^+ = -2k_t\sqrt{t}(-A_1 + 2MA_4) \tag{A14a}$$

$$\widehat{T}_{01}^- = -4p_t k_t(A_1 + tA_2) \tag{A14b}$$

$$\widehat{T}_{11}^+ = -2k_t(2MA_1 - tA_4) \tag{A14c}$$

$$\widehat{T}_{11}^- = \;\;\; 4p_t k_t\sqrt{t}A_3 \tag{A14d}$$

The quantum numbers of the PCHAs are best computed using the standard non relativistic state $|J, M, L, S\rangle$, cf. Appendix of Ref. [28]. Using Eq. (B5) from [29], we can express the 2-nucleon state $|J, M; \lambda_4, \lambda_2\rangle$ as

$$\sqrt{2}|J,0;\pm\pm\rangle = \pm |J,0,J,0\rangle$$

$$+ \left(\frac{J}{2J+1} \right)^{\frac{1}{2}} |J,0,J-1,1\rangle$$

$$- \left(\frac{J+1}{2J+1} \right)^{\frac{1}{2}} |J,0,J+1,1\rangle, \tag{A15a}$$

$$\sqrt{2}|J,\pm 1;\pm\mp\rangle = \mp |J,\pm 1,J,1\rangle$$

$$+ \left(\frac{J+1}{2J+1} \right)^{\frac{1}{2}} |J,\pm 1,J-1,1\rangle$$

$$+ \left(\frac{J}{2J+1} \right)^{\frac{1}{2}} |J,\pm 1,J+1,1\rangle. \tag{A15b}$$

Since $|J, M, L, S\rangle$ have parity $(-1)^{L+1}$ and charge conjugation $(-1)^{L+S}$, the PCHAs are invariant under CP. In the above decomposition, only $|J,0,J,0\rangle$ has $CP = -1$.

Introducing standard combinations of invariant amplitudes, we find that their quantum numbers are

$$F_1 = -A_1 + 2MA_4, \quad \eta = +1, \quad CP = +1, \quad \text{(A16a)}$$
$$F_2 = A_1 + tA_2, \quad \eta = -1, \quad CP = -1, \quad \text{(A16b)}$$
$$F_3 = 2MA_1 - tA_4, \quad \eta = +1, \quad CP = +1, \quad \text{(A16c)}$$
$$F_4 = A_3, \quad \eta = -1, \quad CP = +1. \quad \text{(A16d)}$$

Appendix B: $s-$channel helicity amplitudes and observables

We are interested in the observables for the photoproduction of a neutral pion at the leading order in the center of mass energy squared. The observables are functions of the $s-$channel amplitudes, defined by

$$A^s_{\mu_4,\mu_2\mu_1} = \bar{u}_{\mu_4}(p_4) \sum_{i=1}^{4} A_i M_i \, u_{\mu_2}(p_2). \quad \text{(B1)}$$

In Walker's notation [15] we have ($W = \sqrt{s}$)

$$A^s_{+,+1} = (8\pi W)H_4, \quad A^s_{+,-1} = (8\pi W)H_3, \quad \text{(B2a)}$$
$$A^s_{-,-1} = (8\pi W)H_1, \quad A^s_{-,+1} = (8\pi W)H_2. \quad \text{(B2b)}$$

H_1 and H_4 are single spin flip amplitudes, H_2 is the non-flip amplitude and H_3 is the double flip amplitude.

We use SAID/MAID conventions for the observables [30]

$$\frac{d\sigma}{dt} = \frac{\pi}{k_s^2} \frac{1}{2} \left(|H_1|^2 + |H_2|^2 + |H_3|^2 + |H_4|^2 \right), \quad \text{(B3a)}$$

$$\Sigma \frac{d\sigma}{dt} = \frac{\pi}{k_s^2} \operatorname{Re}\left(H_1 H_4^* - H_2 H_3^* \right), \quad \text{(B3b)}$$

$$T \frac{d\sigma}{dt} = \frac{\pi}{k_s^2} \operatorname{Im}\left(H_1 H_2^* + H_3 H_4^* \right), \quad \text{(B3c)}$$

$$R \frac{d\sigma}{dt} = \frac{\pi}{k_s^2} \operatorname{Im}\left(H_3 H_1^* + H_4 H_2^* \right). \quad \text{(B3d)}$$

$k_s = (s-M^2)/2\sqrt{s} = ME_\gamma/\sqrt{s}$ is the photon momentum in the s-channel center of mass frame.

The $s-$channel amplitudes can be evaluated using an explicit representation for the spinors as we did in the previous section. In the $s-$channel region, the four vector are

$$k^\mu = (k_s, 0, 0, \ k_s), \quad q^\mu = (E^s_\pi, \ q_s \sin\theta_s, 0, \ q_s \cos\theta_s),$$
$$p_2^\mu = (E_2^s, 0, 0, -k_s), \quad p_4^\mu = (E_4^s, -q_s \sin\theta_t, 0, -q_s \cos\theta_t). \quad \text{(B4)}$$

The kinematical quantities are

$$k_s = (s - M^2)/2\sqrt{s}, \quad E_\pi^s = (s - M^2 + \mu^2)/2\sqrt{s},$$
$$E_1^s = (s + M^2)/2\sqrt{s}, \quad E_2^s = (s + M^2 - \mu^2)/2\sqrt{s},$$
$$\cos\theta_s = \frac{t - u + \Delta/s}{4k_s q_s}, \quad \sin\theta_s = \frac{\sqrt{\phi/s}}{2k_s q_s}, \quad \text{(B5)}$$

with $\Delta = M^2(M^2 - \mu^2)$ and

$$q_s = \left[(s - (M+\mu)^2)(s - (M-\mu)^2) \right]^{\frac{1}{2}} / 2\sqrt{s}. \quad \text{(B6)}$$

For the evaluation of Eq. (B1), the spinors are

$$u_+(p_2) = \begin{pmatrix} \sqrt{E_2^s + M} \ \chi_2(0) \\ \sqrt{E_2^s - M} \ \chi_2(0) \end{pmatrix},$$
$$u_-(p_2) = \begin{pmatrix} -\sqrt{E_2^s + M} \ \chi_1(0) \\ \sqrt{E_2^2 - M} \ \chi_1(0) \end{pmatrix}, \quad \text{(B7)}$$
$$\bar{u}_+(p_4) = \left(\sqrt{E_4^2 + M} \ \chi_2^\dagger(\theta_s) \ \ -\sqrt{E_4^s - M} \ \chi_2^\dagger(\theta_s) \right),$$
$$\bar{u}_-(p_4) = \left(\sqrt{E_4^s + M} \ \chi_1^\dagger(\theta_s) \ \ \sqrt{E_4^s - M} \ \chi_1^\dagger(\theta_s) \right),$$

and the polarization tensor for the photon is $\epsilon^\mu(k, \pm 1) = (0, \mp 1, -i, 0)/\sqrt{2}$.

The expression for the $s-$channel helicity amplitudes in terms of the CGLN invariant amplitudes A_i are quite lengthy. Their expressions are most conveniently expressed as function of other scalar amplitudes, the CGLN $\mathcal{F}_i$. We obtain

$$H_1 = \frac{-1}{\sqrt{2}} \sin\theta_s \cos\frac{\theta_s}{2} \left(\mathcal{F}_3 + \mathcal{F}_4 \right) \quad \text{(B8a)}$$

$$H_3 = \frac{1}{\sqrt{2}} \sin\theta_s \sin\frac{\theta_s}{2} \left(\mathcal{F}_3 - \mathcal{F}_4 \right) \quad \text{(B8b)}$$

$$H_2 = \sqrt{2} \cos\frac{\theta_s}{2} \left(\mathcal{F}_2 - \mathcal{F}_1 \right) + H_3 \quad \text{(B8c)}$$

$$H_4 = \sqrt{2} \sin\frac{\theta_s}{2} \left(\mathcal{F}_2 + \mathcal{F}_1 \right) - H_1 \quad \text{(B8d)}$$

where

$$\mathcal{F}_1 = \frac{Z_2^+ Z_4^+}{8\pi W} \left[-(M - W)A_1 + \frac{\mu^2 - t}{2}(A_3 - A_4) + (M - W)^2 A_4 \right] \quad \text{(B9a)}$$

$$\mathcal{F}_2 = \frac{Z_2^- Z_4^-}{8\pi W} \left[-(M + W)A_1 + \frac{\mu^2 - t}{2}(A_3 - A_4) + (M + W)^2 A_4 \right] \quad \text{(B9b)}$$

$$\mathcal{F}_3 = q_s \frac{Z_2^- Z_4^+}{8\pi W} (M + W) \left[-(M - W)A_2 + (A_3 - A_4) \right] \quad \text{(B9c)}$$

$$\mathcal{F}_4 = q_s \frac{Z_2^+ Z_4^-}{8\pi W} (M + W) \left[-(M + W)A_2 + (A_3 - A_4) \right] \quad \text{(B9d)}$$

It worth noting that the amplitudes $\mathcal{F}_i$ have kinematical singularities coming from the factors

$$Z_{2,4}^\pm = \sqrt{E_{2,4} \pm M}. \quad \text{(B10)}$$

Another instructive method to obtain the $s-$channel amplitudes, given n [27], is to express them in terms of

the $t-$channel using crossing relations. Of course, parity conserving combinations rotate independently

$$\begin{pmatrix} A^s_{+,+1} \pm A^s_{-,-1} \\ A^s_{+,-1} \mp A^s_{-,+1} \end{pmatrix} = -iR \left(\frac{\chi_2 \mp \chi_4}{2} \right) \begin{pmatrix} A^t_{+,+1} \pm A^t_{-,-1} \\ A^t_{+-,1} \mp A^t_{-+,1} \end{pmatrix}.$$
(B11)

The rotation matrix is

$$R(\chi) = \begin{pmatrix} \cos\chi & \sin\chi \\ -\sin\chi & \cos\chi \end{pmatrix},$$
(B12)

and the crossing angles are

$$\cos\chi_2 = -\frac{-st + M^2(\mu^2 - t)}{\lambda^{\frac{1}{2}}(s,0,M^2)\lambda^{\frac{1}{2}}(t,0,\mu^2)} \approx -\sqrt{\frac{-t}{4M^2 - t}},$$
$$\cos\chi_4 = \frac{(-t)(s-\mu^2) - M^2(t+2\mu^2)}{\lambda^{\frac{1}{2}}(s,\mu^2,M^2)\lambda^{\frac{1}{2}}(t,M^2,M^2)} \approx \sqrt{\frac{-t}{4M^2 - t}}.$$
(B13)

The symbols $\approx$ stands for the leading order in s and the triangle function is $\lambda(a,b,c) = a^2 + b^2 + c^2 - 2(ab + bc + ca)$. Since the crossing matrix (B11) is a rotation (up to a global phase[2]), it preserves the norm. The differential cross section can be then computed directly with the $t-$channel amplitudes without performing the rotation. The result is

$$\frac{d\sigma}{dt} = \frac{1}{64\pi} \frac{|k_t|^2}{4M^2 E_\gamma^2} \Big[\ 2|\sin\theta_t|^2 \left(|2p_t F_2|^2 - t|F_1|^2 \right)$$
$$+ (1 - \cos\theta_t)^2 \left| F_3 + 2\sqrt{t}p_t F_4 \right|^2$$
$$+ (1 + \cos\theta_t)^2 \left| F_3 - 2\sqrt{t}p_t F_4 \right|^2 \Big].$$
(B14)

In the evaluation of the differential cross section with $t-$channel amplitudes, one has to remember that $\sin\theta_t$ is a complex number in the physical region of the process $\gamma p \to \pi^0 p$.

Single polarization observables Σ, T, R are best evaluated in the high energy limit. The error made by using this approximation are compensated by calculating the ratio of quadratic forms of amplitudes, cf. Eq. (B3). Keeping only the dominant term in s, the crossing relations take a simple form

$$\frac{1}{\sqrt{2}} \begin{pmatrix} H_4 + H_1 \\ H_3 - H_2 \end{pmatrix} \approx \frac{W/8\pi}{4M^2 - t} \begin{pmatrix} 2M & \sqrt{-t} \\ -\sqrt{-t} & 2M \end{pmatrix} \begin{pmatrix} \sqrt{-t}F_1 \\ F_3 \end{pmatrix},$$
$$\frac{1}{\sqrt{2}} \begin{pmatrix} H_4 - H_1 \\ H_3 + H_2 \end{pmatrix} \approx \frac{W}{8\pi} \begin{pmatrix} 0 & 1 \\ -1 & 0 \end{pmatrix} \begin{pmatrix} F_2 \\ \sqrt{-t}F_4 \end{pmatrix}.$$
(B15)

The apparent pole at $t = 4M^2$ in the first equation above is spurious and disappears when the scalar amplitudes A_i are substituted. We indeed obtain

$$\frac{1}{\sqrt{2}} \begin{pmatrix} H_4 + H_1 \\ H_3 - H_2 \end{pmatrix} \approx \frac{W}{8\pi} \begin{pmatrix} \sqrt{-t}A_4 \\ A_1 \end{pmatrix}.$$
(B16)

The relations (B15) were derived in Ref. [14]. We corrected a sign mistake in the rotation matrix Eq. (2.3) in Ref. [14]. This mistake propagated through the observables. The reader could easily check that the pole $t = 4M^2$ does not cancel as it should in the observables Eq. (A.10)-(A.13) in Ref. [14]. The correct expressions at leading order in the energy squared are

$$\frac{d\sigma}{dt} \approx \frac{1}{32\pi} \left[\frac{|F_3|^2 - t|F_1|^2}{4M^2 - t} + |F_2|^2 - t|F_4|^2 \right] \quad \text{(B17a)}$$

$$\Sigma\frac{d\sigma}{dt} \approx \frac{1}{32\pi} \left[\frac{|F_3|^2 - t|F_1|^2}{4M^2 - t} - |F_2|^2 + t|F_4|^2 \right] \quad \text{(B17b)}$$

$$T\frac{d\sigma}{dt} \approx \frac{1}{16\pi} \sqrt{-t} \ \text{Im} \left[\frac{F_3 F_1^*}{4M^2 - t} + F_4 F_2^* \right] \quad \text{(B17c)}$$

$$R\frac{d\sigma}{dt} \approx \frac{1}{16\pi} \sqrt{-t} \ \text{Im} \left[\frac{F_3 F_1^*}{4M^2 - t} - F_4 F_2^* \right] \quad \text{(B17d)}$$

---

[1] A.C. Irving and R.P. Worden. Regge Phenomenology. *Phys.Rept.*, 34:117–231, 1977.

[2] R. Worden. Regge models of forward pion and eta photoproduction. *Nucl.Phys.*, B37:253–312, 1972.

[3] CLAS collaboration. in preparation.

[4] R. Odorico. A Critical Study of Finite Energy Sum Rule Difficulties in Pion Photoproduction. *Nucl.Phys.*, B101:480, 1975.

[5] D. Drechsel, S.S. Kamalov, and L. Tiator. Unitary Isobar Model - MAID2007. *Eur.Phys.J.*, A34:69–97, 2007.

[6] Ron L. Workman, William J. Briscoe, Mark W. Paris, and Igor I. Strakovsky. Updated SAID analysis of pion photoproduction data. *Phys.Rev.*, C85:025201, 2012.

[7] A.V. Anisovich, R. Beck, E. Klempt, V.A. Nikonov, A.V. Sarantsev, et al. Pion- and photo-induced transition amplitudes to ΛK, ΣK, and $N\eta$. *Eur.Phys.J.*, A48:88, 2012.

[8] H. Kamano, S.X. Nakamura, T. S. H. Lee, and T. Sato. Nucleon resonances within a dynamical coupled-channels model of πN and γN reactions. *Phys.Rev.*, C88(3):035209, 2013.

[9] Vladimir N. Gribov, Yuri L. Dokshitzer, and Julia Nyiri. Strong interactions of hadrons at high emnergies: Gribov lectures on. 2009.

[10] G.F. Chew, M.L. Goldberger, F.E. Low, and Yoichiro Nambu. Relativistic dispersion relation approach to photomeson production. *Phys.Rev.*, 106:1345–1355, 1957.

---

[2] This phase is present in the original calculation in Ref. [27] but was overlooked in subsequent publications. See for instance Ref. [11].

[11] P.D.B. Collins. *Regge Theory and High Energy Physics.* Cambridge Monograph on Mathematical Physics, 1977.

[12] A.D. Martin and Spearman T. D. *Elementary Particle Theory.* Noth-Holland, 1970.

[13] J.P. Ader, M. Capdeville, and Ph. Salin. *Nucl. Phys.*, B3:407, 1967.

[14] I.S. Barker, A. Donnachie, and J.K. Storrow. Analysis of pi0 Photoproduction at Intermediate and High-Energy. *Nucl.Phys.*, B79:431, 1974.

[15] R.L. Walker. Phenomenological analysis of single pion photoproduction. *Phys.Rev.*, 182:1729–1748, 1969.

[16] P.D.B. Collins. Regge theory and particle physics. *Phys.Rept.*, 1:103–234, 1971.

[17] Byung Geel Yu, Tae Keun Choi, and W. Kim. Regge phenomenology of pion photoproduction off the nucleon at forward angles. *Phys.Rev.*, C83:025208, 2011.

[18] Robert L. Anderson, D. Gustavson, J.R. Johnson, I. Overman, D. Ritson, et al. HIGH-ENERGY pi0 PHOTOPRODUCTION FROM HYDROGEN WITH UNPOLARIZED AND LINEARLY POLARIZED PHOTONS. *Phys.Rev.*, D4:1937, 1971.

[19] B. Barish, R. Gomez, D. Kreinick, C. Peck, J. Pine, et al. pi0 and rho0 Photoproduction from 6-GeV to 18-GeV. *Phys.Rev.*, D9:566, 1974.

[20] G.C. Bolon, C. Garelick, S. Homma, R. Lewis, W. Lobar, et al. MEASUREMENTS OF PI0 PHOTOPRODUCTION CROSS-SECTIONS FOR INCIDENT GAMMA-RAY ENERGIES OF 2.0-Gev/c TO 5.0-Gev/c. *Phys.Rev.Lett.*, 18:926, 1967.

[21] W. Braunschweig, H. Dinter, W. Erlewein, H. Frese, K. Luebelsmeyer, et al. Single photoproduction of neutral pi mesons on deuterium in the forward direction at 4 gev. *Nucl.Phys.*, B51:157–166, 1973.

[22] P.S.L. Booth, G.R. Court, B. Craven, R. Gamet, P.J. Hayman, et al. Polarized target asymmetry for pi-zero photoproduction at 4 gev. *Phys.Lett.*, B38:339–341, 1972.

[23] H. Bienlein, W. Braunschweig, H. Dinter, W. Erlewein, H. Frese, et al. Target asymmetry for neutral pi meson photoproduction on polarized protons at 4 gev in the forward direction. *Phys.Lett.*, B46:131–134, 1973.

[24] M. Deutsch, L. Golub, P. Kijewski, D. Potter, D.J. Quinn, et al. Recoil-proton polarization in neutral-pion photoproduction and in proton Compton scattering. *Phys.Rev.Lett.*, 29:1752–1755, 1972.

[25] A.M. Osborne, A. Brownam, K. Hanson, W.T. Meyer, A. Silverman, et al. Pi0 photoproduction from neutrons. *Phys.Rev.Lett.*, 29:1621–1624, 1972.

[26] M.R. Pennington. SPQR - Spectroscopy: Prospects, Questions and Results. *EPJ Web Conf.*, 73:01001, 2014.

[27] T.L. Trueman and G.C. Wick. Crossing relations for helicity amplitudes. *Annals Phys.*, 26:322–335, 1964.

[28] R.W. Childers and W. G. Hollady. Regge Poles and the Photoproduction of Pions. *Phys.Rev.*, 132:1809–1818, 1963.

[29] M. Jacob and G.C. Wick. On the general theory of collisions for particles with spin. *Annals Phys.*, 7:404–428, 1959.

[30] R.L. Workman, M.W. Paris, W.J. Briscoe, L. Tiator, S. Schumann, et al. Model dependence of single-energy fits to pion photoproduction data. *Eur.Phys.J.*, A47:143, 2011.